



Trans. Nonferrous Met. Soc. China 33(2023) 3797-3811

Transactions of Nonferrous Metals Society of China

www.tnmsc.cn



Effects of deposition temperature on microstructures and ablative properties of SiC coatings prepared by CVD from methylsilane

Xiang-long HU¹, Xiao LUO¹, Xin YANG¹, Rui-xuan TAN², Qi-zhong HUANG¹

- 1. National Key Laboratory of Science and Technology on High-strength Structural Materials, Central South University, Changsha 410083, China;
- 2. Hunan Provincial Key Laboratory for Advanced Carbon Materials and Applied Technology, Hunan University, Changsha 410082, China

Received 11 May 2022; accepted 31 October 2022

Abstract: Using the methylsilane (MS) as a gas precursor, SiC coatings were prepared on the surface of graphite by the chemical vapor deposition (CVD) method at different deposition temperatures. The effects of temperature on the deposition rate, microstructures and ablative properties of SiC coatings were investigated systematically. The results showed that the SiC deposition rate of SiC coating using MS at $1000\,^{\circ}$ C was $50-120\,\mu\text{m/h}$, which was much higher than that using methyltrichlorosilane ($5-10\,\mu\text{m/h}$). The SiC coatings deposited at lower temperatures ($900-1000\,^{\circ}$ C) exhibited smooth and spherical compact packing morphology, while the SiC coatings deposited at higher temperatures ($1100-1200\,^{\circ}$ C) appeared to possess an irregular cauliflower morphology with an significantly increased size of SiC particles. Therefore, the SiC coating prepared at deposition temperature of $1000\,^{\circ}$ C had suitable density, roughness, and uniform size of coating microstructure. Meanwhile, the mass ablation rate and linear ablation rate of the obtained SiC coating were respectively $0.0096\,\text{mg/s}$ and $0.3750\,\mu\text{m/s}$ after plasma ablation at $2300\,^{\circ}$ C for $80\,\text{s}$, exhibiting excellent ablative resistance. This study provided a theoretical and technical foundation for the preparation of SiC coating using the MS as the gas precursor by the CVD method.

Key words: methylsilane; chemical vapor deposition; SiC coating; deposition temperature; microstructure; ablative properties

1 Introduction

SiC has excellent high-temperature mechanical properties and stability, relatively high thermal conductivity, low thermal expansion coefficient, as well as anti-radiation properties, which can prevent the oxidation and ablation functionalities for C/C composites below 1700 °C [1–5]. Therefore, SiC coatings have been extensively studied in aerospace, microelectronics, nuclear energy and other fields [6–9]. Especially, the SiC coating on the carbon materials would be beneficial to obtaining the high thermal conductivity and suitable electrical

insulation, which has become the focus of semiconductor research about using as thermal conductive fillers for electronic packaging materials [10]. Among various SiC coating methods, chemical vapor deposition (CVD) is a fabrication strategy of great importance [11–13]. The SiC coatings prepared by CVD may possess different crystal structures, morphologies and orientations, depending on various processing parameters [14,15].

As a new type of raw material, methylsilane (MS) has significant advantages such as low deposition temperature, fast deposition rate, good diffusivity, and no chemical corrosion. On the one hand, the SiC coating with good performance can

be obtained at lower temperatures (650–800 °C) using MS as raw material, and the deposition rate is 10-20 times that of methyltrichlorosilane (MTS) as a raw material under the same conditions (MTS isothermal deposition rate is $5-10 \mu m/h$). On the other hand, the preparation process of SiC coatings by CVD from MS is a safe and environmentally friendly process, with no corrosive chlorinecontaining by-products (HCl and silicon-chlorine compounds) formed [16,17]. Previous research showed that the process parameters such as temperature, pressure, flow rate and carrier gas/ precursor ratio, significantly affect the quality of SiC coating [18,19], and the deposition temperature has a greater effect on the microstructure of SiC coatings. In addition, the deposition temperature has a significant effect on the deposition rate of SiC coatings, and the deposition rate has an impact on the coating quality [20]. Generally, the excessive deposition rate will prevent complete fusion or annexation of SiC grains, affecting the oxidation and ablation resistances of the SiC coatings. So, it is of great significance to investigate the effect of deposition temperature, deposition rate on the microstructure and ablative properties of SiC coating prepared by CVD from MS.

In this work, the deposition temperatures of SiC coatings prepared by CVD from MS were set in the range of 900–1200 °C. Firstly, the deposition mechanism and pyrolysis process of MS were analyzed. Secondly, the ablation behavior of CVD-SiC coatings from MS was evaluated by plasma flame for 80 and 120 s, respectively. Microstructures of SiC coatings before and after ablation were comparatively investigated. Finally, the ablation resistance mechanism of CVD-SiC coatings from MS was discussed. Therefore, this study presents a reliable way to fabricate high quality of SiC coating and provides the mechanism model to understand ablation resistance for CVD-SiC coatings.

2 Experimental

2.1 CVD-SiC coatings from MS

A hot-wall vertical vacuum reactor, with an effective cylindrical deposition space of $d300 \text{ mm} \times 500 \text{ mm}$ was employed. The substrates, i.e., high-purity graphite sheets with the size of $40 \text{ mm} \times 40 \text{ mm} \times 3 \text{ mm}$ (length × width × thickness), were

suspended at a certain height (the graphite substrate was 30 mm away from the gas distribution plate at the bottom of the furnace) by molybdenum wire. MS (CH₃SiH₃) was used as SiC precursor. The flow rate ratio of MS to H₂ was 1.2:8. Deposition temperatures were from 900 to 1200 °C, deposition pressure was 120 Pa, and reaction time was 1 or 2 h. The SiC coatings deposited at 900-1200 °C for 1 h were labeled as SiC-900-1, SiC-1000-1, SiC-1100-1 and SiC-1200-1, respectively. The SiC coatings deposited at 900-1200 °C for 2 h were labeled SiC-900-2, SiC-1000-2, SiC-1100-2 SiC-1200-2, respectively. SiC with a Si/C molar ratio of 1:1 could be obtained with no aggressive chlorine-containing compounds formed.

2.2 Ablation test

Multiplaz 3500 water-stable plasma ablation equipment was used to test the ablation properties of CVD-SiC coatings. During ablation process, the distance between the muzzle and the center of the sample was 20 mm, the ablation direction of the flame was perpendicular to the coating surface, and the temperature at the center of the sample was about 2300 °C.

The ablation performance of the sample was evaluated by the mass and linear ablation rates before and after ablation. And the formulas for calculating the mass and linear ablation rates of the coating are as follows:

$$R_{\rm m} = (m_0 - m_t)/t \tag{1}$$

$$R_1 = (l_0 - l_t)/t \tag{2}$$

where $R_{\rm m}$ and $R_{\rm l}$ are the mass and linear ablation rates, respectively; m_0 and m_t are the mass of the sample before and after ablation, respectively; l_0 and l_t are the thickness at ablation center of the sample before and after ablation, respectively; t is the test time.

2.3 Characterization

The as-prepared and ablated coatings were analyzed by X-ray diffraction (XRD, Rigaku, Japan), with Cu K_{α} (λ =1.54056 Å) light source and scanning range of 20°–80°. The microstructure and cross-section microstructure of the coating were characterized by scanning electron microscopy (SEM, JSM-7610FPlus, Japan) equipped with energy dispersive spectrometer (EDS).

3 Results and discussion

3.1 Pyrolysis process of MS and deposition mechanism

Experimental and theoretical studies show that the main reaction paths and surface activity components play an important role in the deposition. The overall reaction of MS pyrolysis process is as follows:

$$CH_3SiH_3(g) \rightarrow SiC(s) + 3H_2(g)$$
 (3)

During CVD process, the pyrolysis of MS and formation of SiC coating are a complex gas-solid chemical reaction course. The decomposition of MS and the generation of intermediate gaseous products can significantly affect the CVD process. The gas phase reactions in the CVD process of MS-H₂ system can be mainly summarized as follows [21–24]:

- (1) Splitting of C—H or Si—H bond causes the decomposition of MS and generates the intermediate methylsilyl radical $HSiCH_3$ (or H_2Si — CH_2) and hydrogen.
- (2) Splitting of Si—C bond can generate gaseous CH₄ and SiH₂.
- (3) The formed intermediate hydrocarbon (HSiCH₃ or H₂Si=CH₂) with other gaseous products generate SiC crystals and by-products.

The main reactions concerned in the CVD process are listed as follows:

$$CH_3SiH_3(g) \rightarrow$$

$$HSiCH_3(g)$$
 (or $H_2Si=CH_2(g))+H_2(g)$ (4)

$$CH_3SiH_3(g) \rightarrow CH_4(g) + SiH_2(g)$$
 (5)

 $CH_3SiH_3(g)+SiH_2(g) \rightarrow$

$$HSiCH_3(g)$$
 (or $H_2Si=CH_2(g)$)+ $SiH_4(g)$ (6)

$$HSiCH_3(g)$$
 (or $H_2Si=CH_2(g))\rightarrow SiC(s)+2H_2(g)$ (7)

$$CH_4(g) \rightarrow C(s) + 2H_2(g)$$
 (8)

$$SiH_4(g) \rightarrow Si(s) + 2H_2(g)$$
 (9)

$$C(s)+Si(s) \rightarrow SiC(s)$$
 (10)

JOHNSON et al [25] studied the decomposition process of MS and conformed that Reaction (4) has the lowest activation energy and the reaction leading to HSiCH₃ has the largest pre-exponential factor. Therefore, Reaction (4) is the dominant decomposition path for MS, which is also consistent with the formation of the isomeric intermediates HSiCH₃ or H₂Si=CH₂. Meanwhile, the detection of dominant H₂ in the mass

spectrometry results can be mainly attributed to the occurrence of Reaction (4). Moreover, SANCHEZ and SIBENER [26] and OHSHITA [27] demonstrated that participation of different species of isomeric HSiCH₃ and H₂Si=CH₂ is important for SiC crystal growth, and reactions of these molecules determine the CVD growth rate. Meanwhile, previous studies [28,29] reported that the yield of HSiCH₃ as the primary product was about 98% in the homogeneous gas phase decomposition of MS at 700 °C. However, as the temperature was elevated to 900 °C, the formed HSiCH₃ was reduced to 70%. The above results were in accordance with the partial pressure analyses of mass spectrometry [25,29–31], which verified that the isomeric intermediates HSiCH₃ and H₂Si=CH₂ are the primary products of MS decomposition and the dominant decomposition path for MS at 650-1000 °C is Reaction (4). Therefore, HSiCH₃ and H₂Si=CH₂ are the dominant molecules that participate in growth of SiC coating, and the reactions of these molecules determine the growth rate, microstructure and phase composition of the coating.

The physical changes and chemical reactions involved in the CVD process are complex. However, the deposition process based on the pyrolysis and decomposition results of MS can be summarized as follows [21-31]: (1) MS flows into the deposition chamber with hydrogen for decomposition reaction; (2) The hydrocarbon intermediate gaseous products formed by the reaction diffuse to the surface of the substrate; (3) The intermediate gaseous active molecules (atoms) are adsorbed on the surface of the substrate; (4) The gaseous products adsorbed on the substrate surface react further and form initial crystal nuclei; (5) The grains generated by nucleation constantly merge and grow to form a continuous coating skeleton; (6) Residual gaseous reaction by-products are separated from the deposition surface and discharged from deposition chamber; (7) The deposited SiC grains continue to fill in the skeleton pores, further forming a continuous dense coating, and with the extension of deposition time, the dense SiC coating gradually thickens.

3.2 Effect of deposition temperature on microstructure and phase composition of CVD-SiC coatings prepared from MS

Figure 1 shows the phase analysis results of

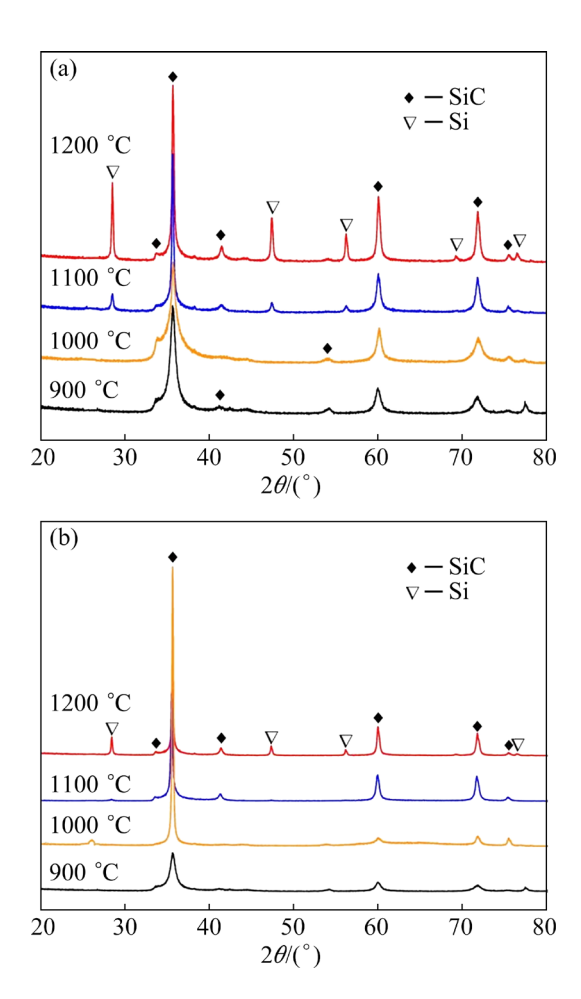


Fig. 1 XRD patterns of SiC coatings deposited at different temperatures for 1 h (a) and 2 h (b)

the SiC coatings deposited at different temperatures for different time. The phase composition of SiC coatings prepared at different temperatures differs significantly. At low temperatures (900 and 1000 °C), the coatings are mainly composed of a single SiC phase. The diffraction peaks at 2θ of 35.7° , 60.0° and 71.5° correspond to the (111), (220), (311) crystal planes of SiC, respectively. Among them, the diffraction peak at 35.7° is the strongest, indicating that SiC grows along the most densely packed (111) crystal plane during the deposition process, and the (111) plane has a strong preferred orientation. However, as the deposition temperature rises to 1100 °C, a relatively weak free Si peak appears in the coating. When the deposition temperature rises to 1200 °C, the free Si diffraction peak becomes stronger. In addition, with the increase of deposition temperature, the full width at the half maxima (FWHM) of SiC diffraction peak gradually decreases, indicating that the crystallinity of SiC coating gradually increases. When the deposition time is extended to 2 h, the prepared coating also shows the same phase change trend, which further indicates that the deposition temperature has an important influence on the phase composition of the prepared coating. The formation of free Si in the deposition process is mainly related to the high temperature pyrolysis behavior of MS. Relevant studies showed that when the temperature is higher than 600 °C, MS begins to decompose to produce H₂ [29–31]. When the temperature rises to 700 °C, a small amount of hydrocarbon (C₂H_m and CH₄) is formed in the pyrolysis products. When the temperature increases to 1000 °C, C₃H₆ and SiH₄ appear in pyrolysis products, and the partial pressures of hydrocarbon (C₂H_m and CH₄) increase. As the cracking temperature is higher than 1060 °C, the partial pressure of SiH₄ decreases significantly. At the same time, the partial pressures of hydrocarbon (C_2H_m , CH_4 and C_3H_6) further increase with the increase of temperature. As the deposition temperature increases (≥1100 °C), except for forming SiC, part of the MS cracking intermediates are further cracked to form Si atoms and hydrocarbon (C_2H_m , CH_4 and C_3H_6) [27]. With the progress of the deposition process, the nucleated SiC and Si grains will gradually grow to form a continuous dense coating.

Figures 2 and 3 show the surface morphologies SiC-1000-1, SiC-1100-1 SiC-900-1, SiC-1200-1 coatings. The size of the SiC grains increases gradually with the increase of deposition temperature. At deposition temperature of 900, the SiC coatings are mainly cellular structure with smooth coating surface and the particle size is 15-19 μm (Fig. 3(e)). At 1000 °C, the size of SiC-1000-1 increases to 20–27 μm, and the surface roughness increases as well (Fig. 3(a)). SiC-1100-1 is dominated by large particles of 23-37 µm, with smaller particles of several microns packed between the large grains Figs. 2(e) and (f). The SiC-1200-1 is composed of irregular grains of several microns, forming irregular crystal structure (40 µm) with greatly increased surface roughness (Fig. 2(a)).

The surface morphologies of SiC-900-2, SiC-1000-2, SiC-1100-2 and SiC-1200-2 coatings are shown in Figs. 4 and 5, which are roughly consistent with the law obtained for 1 h deposition (Figs. 2 and 3). With the increase of deposition temperature, the size of SiC particles and the surface roughness of the coating gradually increase.

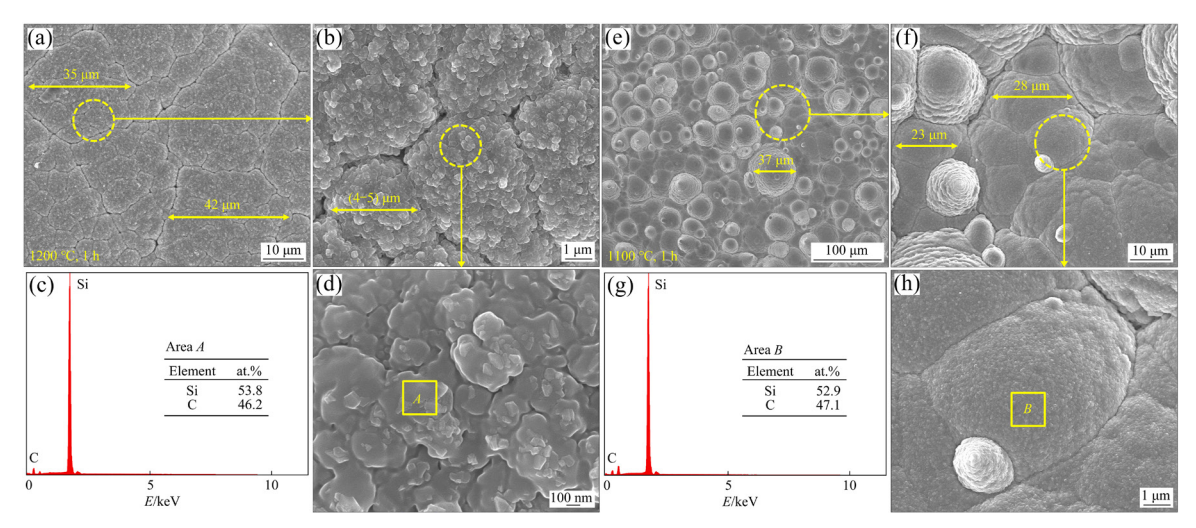


Fig. 2 Surface morphologies by SEM (a, b, d, e, f, h) and EDS data (c, g) of SiC coatings: (a-d) SiC-1200-1; (e-h) SiC-1100-1

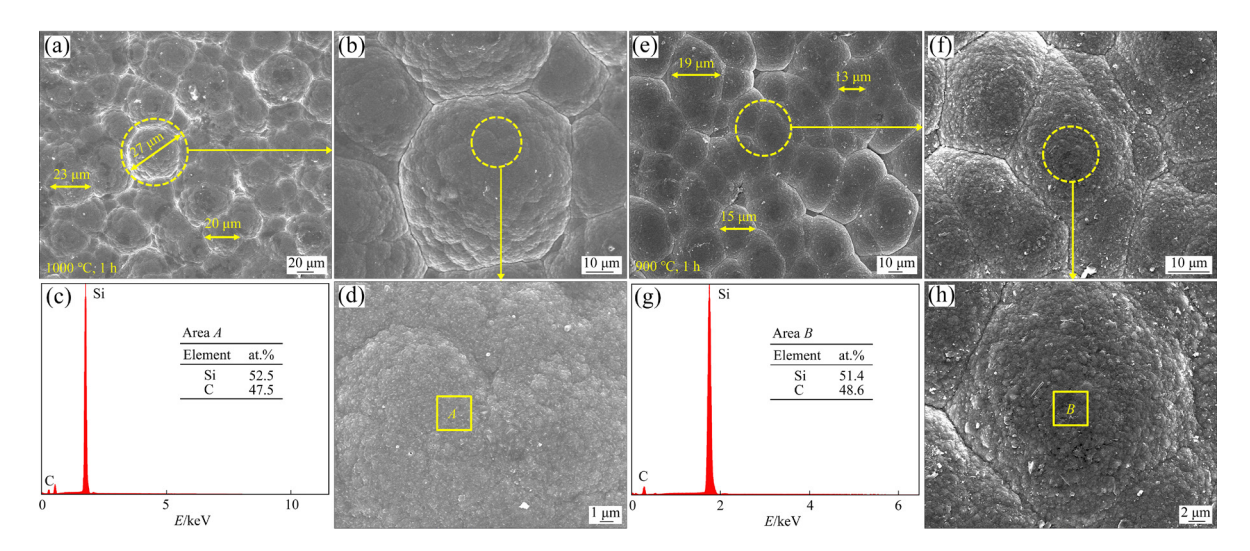


Fig. 3 Surface morphologies by SEM (a, b, d, e, f, h) and EDS data (c, g) of SiC coatings: (a-d) SiC-1000-1; (e-h) SiC-900-1

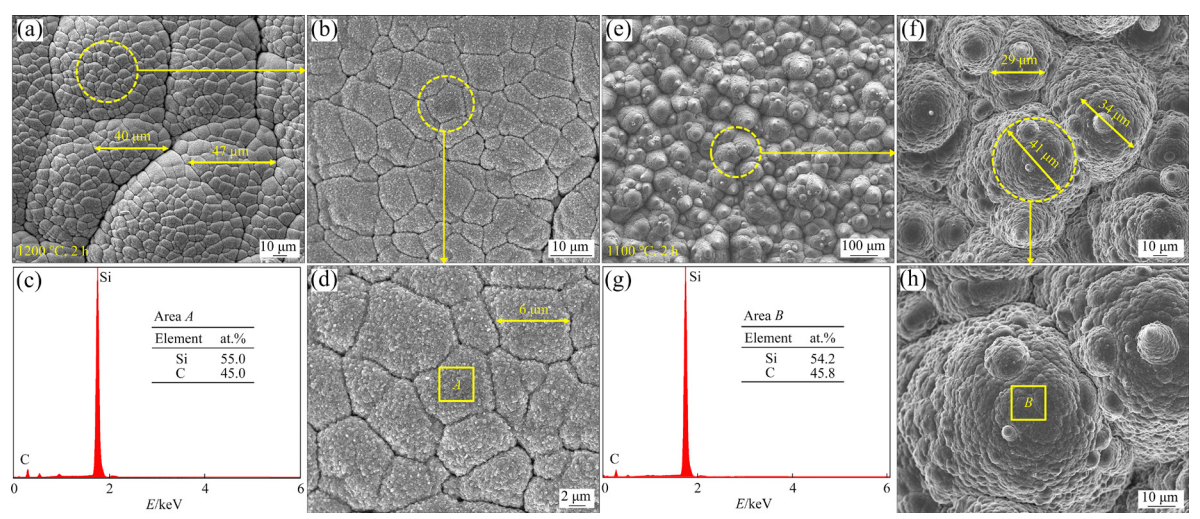


Fig. 4 Surface morphologies by SEM (a, b, d, e, f, h) and EDS data (c, g) of SiC coatings: (a-d) SiC-1200-2; (e-h) SiC-1100-2

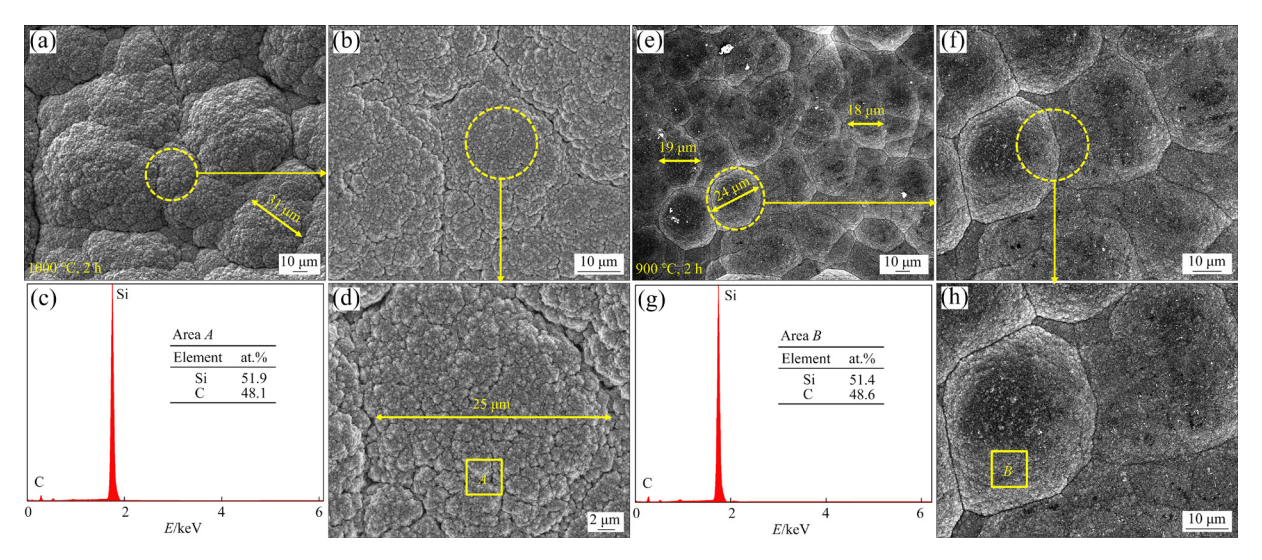


Fig. 5 Surface morphologies by SEM (a, b, d, e, f, h) and EDS data (c, g) of SiC coatings: (a-d) SiC-1000-2; (e-h) SiC-900-2

In the temperature range of 900-1200 °C, the deposition process is controlled by chemical reactions and the deposition rate is accelerated as temperature increases. When the deposition temperature is 900 or 1000 °C, the deposition rate of the coating is relatively slow, the critical nucleation size is small, and the coating surface is dominated by small-sized particles and the coating growth uniformity. As the deposition temperature increases to 1100 and 1200 °C, the deposition rate increases gradually, the growth and fusion of coating particles are enhanced, and the growth rate of the coating is accelerated. The particle size of the coating, the variance of this size and the roughness of the coating increase, while the uniformity of the coating decreases. The morphology of SiC-1200-2 is significantly different from those obtained at lower temperatures (900-1100 °C), which may be due to the high activity of free radicals formed by MS during pyrolysis. With the acceleration of the deposition rate, free Si cannot capture C to form SiC in time, thus Si existing on the surface of the SiC coating forms small particles stacked together.

SiC coatings prepared at different temperatures show different surface morphologies. When the deposition temperature is low (900 and 1000 °C), the coating is smooth, and the SiC exhibits spherical and compact morphology. As deposition temperature increases to 1100 and 1200 °C, the size of SiC crystallites increases significantly, and the SiC particles show an irregular cauliflower-like stacking morphology, which leads to the appearance

of defects such as pores.

During the CVD process, the deposition temperature directly affects the critical nucleation radius and critical nucleation free energy. This has an important impact on the morphology change of SiC grains and the microstructure of the coating. ZHANG et al [32] calculated the critical nucleation radius and critical nucleation free energy in the deposition process, and obtained the following results.

Critical nucleation radius:

$$r_{\rm c} = -2\frac{\gamma}{\Delta G_{\rm v}} \tag{11}$$

Critical nucleation free energy:

$$\Delta G_{v} = \frac{-kT}{\Omega} \ln \left[1 + \exp\left(\frac{\Delta H_{T_g} \Delta T}{RT_g^2}\right) \right]$$
 (12)

Rate of critical nucleus formation:

$$I = z \cdot \exp\left(-\frac{\Delta G^*}{kT}\right) \tag{13}$$

where $r_{\rm c}$ is critical nucleation radius, $\Delta G_{\rm v}$ is critical nucleation free energy, γ is interface energy per unit area, Ω is atomic volume, T is deposition temperature, $T_{\rm g}$ is temperature at which the coating core is in equilibrium with its gas phase, $\Delta T (= T_{\rm g} - T)$ is under-cooling during coating deposition, $\Delta H_{T_{\rm g}}$ is heat of evaporation at vapor phase equilibrium temperature, I is nucleation rate, ΔG^* is system free energy variation, and k, R, and z are constants.

The results show that with the decrease of the deposition temperature, the critical nucleation radius of SiC new phase decreases, the critical nucleation free energy decreases, and rate of critical nucleus formation increases, which is conducive to the formation of uniform fine SiC grains. Thus, the coating deposited at low temperatures presents smooth, flat and compact morphology. However, with the increase of deposition temperature, the critical nucleation radius of SiC new phase gradually increases, and the critical nucleation free energy is also higher. Therefore, when the deposition temperature is high, the SiC grains formed are larger, resulting in rough surface morphology and obvious pore defects between particles.

Figure 6 presents comparison of the thickness

SiC-900-1, SiC-1000-1, SiC-1100-1 and SiC-1200-1 coatings. SiC-900-1 is relatively thin with a thickness of 98 µm. The thickness of the coatings obtained at higher temperatures increases, and the coating growth rate also increases. In the process of SiC deposition, the deposition temperature has positive or negative effects on the deposition rate. Only when the homogeneous reaction of gas phase is too intense, the deposition temperature has negative effects. In the deposition temperature range of 900-1200 °C, the deposition rate increases with the increase of temperature, the positive effect of temperature is greater than the negative effect, and the deposition process is controlled by chemical reaction. Figure 7 shows the SEM-EDS results of SiC-900-2, SiC-1000-2,

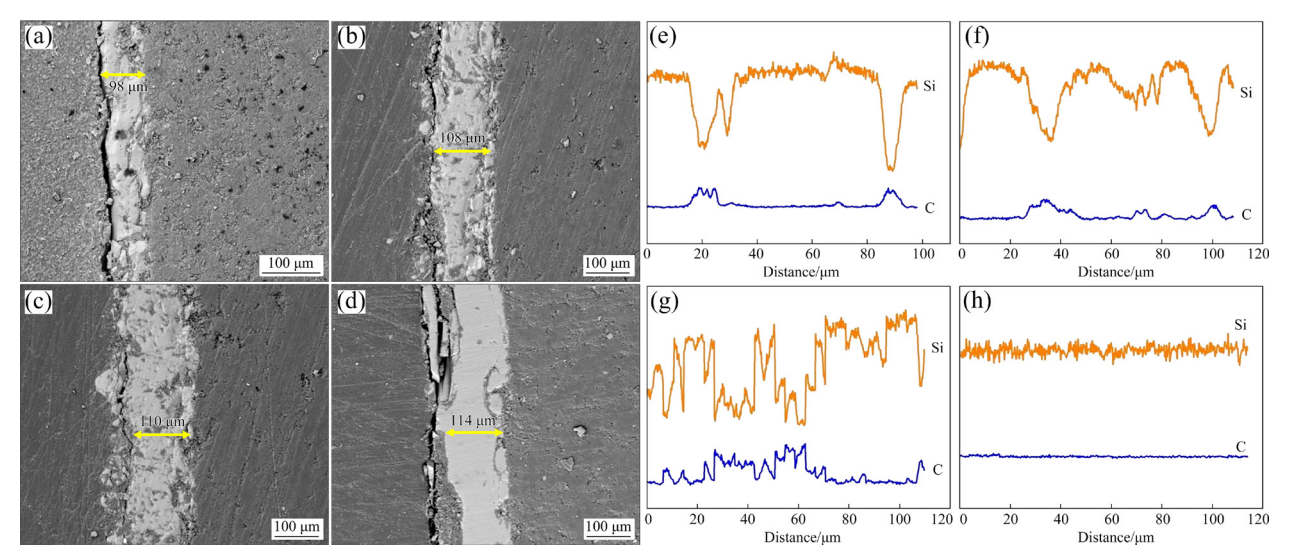


Fig. 6 Fracture microstructures obtained by SEM (a-d) and EDS data (e-h) of SiC coatings: (a, e) SiC-900-1; (b, f) SiC-1000-1; (c, g) SiC-1100-1; (d, h) SiC-1200-1

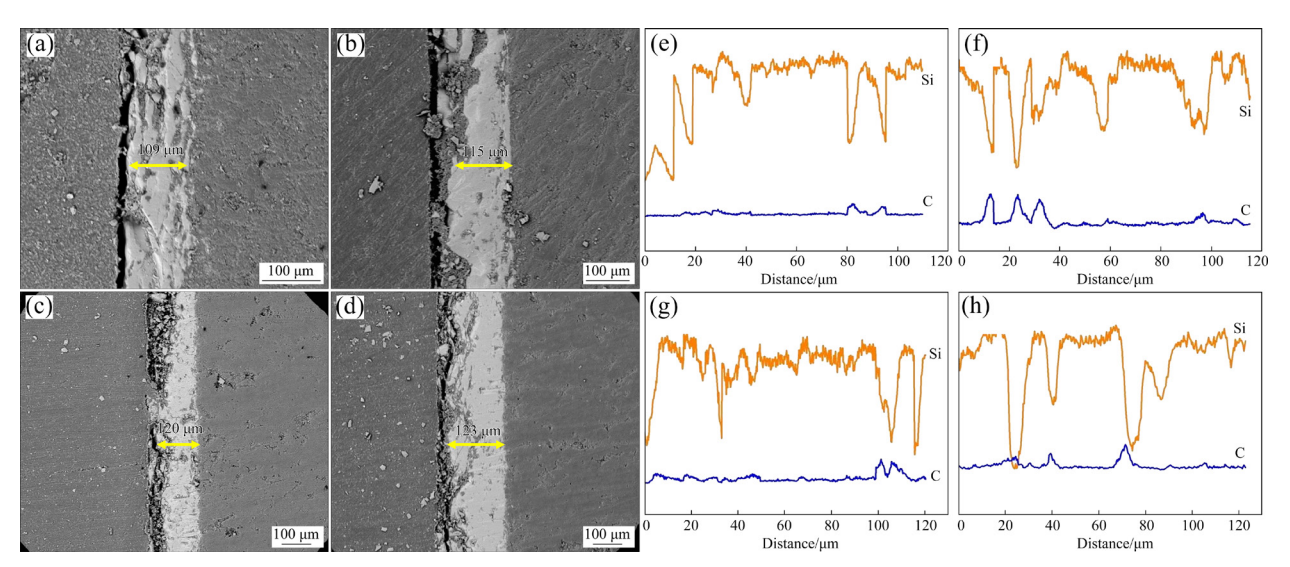


Fig. 7 Fracture microstructures obtained by SEM (a-d) and EDS data (e-h) of SiC coatings: (a, e) SiC-900-2; (b, f) SiC-1000-2; (c, g) SiC-1100-2; (d, h) SiC-1200-2

SiC-1100-2 and SiC-1200-2 coatings. As the deposition time increases, the thickness of the coating does not increase significantly.

The average deposition rate of the coatings at different deposition temperatures is shown in Fig. 8, indicating that the deposition rate remains an upward trend as temperature increases. Although the increase of the deposition temperature can effectively increase the deposition rate of the coating, the coarsening of the SiC grain size is also conducive to the formation of a SiC coating with high crystallinity. However, as SiC grains grow, the roughness of the coating increases. The accumulation gap between the particles also becomes larger. This can lead to the formation of defects, such as pores, and reduce the density of the coating. Therefore, considering the roughness and compactness of SiC coating, the size and crystallinity of the coating, temperature too high or too low is not conducive to the preparation of a coating with excellent comprehensive properties. When the deposition temperature is too low (900 and 1000 °C), the SiC coating with fine grains and compact structure can be obtained. However, the low deposition temperature affects the growth and crystallization process of SiC grain, and reduces the crystallinity of SiC coating. In contrast, excessively high deposition temperatures (1100 and 1200 °C) will reduce the nucleation rate. As a result, the size of the formed grains increases significantly. And a rough and porous coating structure is easily formed after the accumulation of coarse-grained SiC. Therefore, an appropriate deposition temperature must be selected to obtain a specific microstructure.

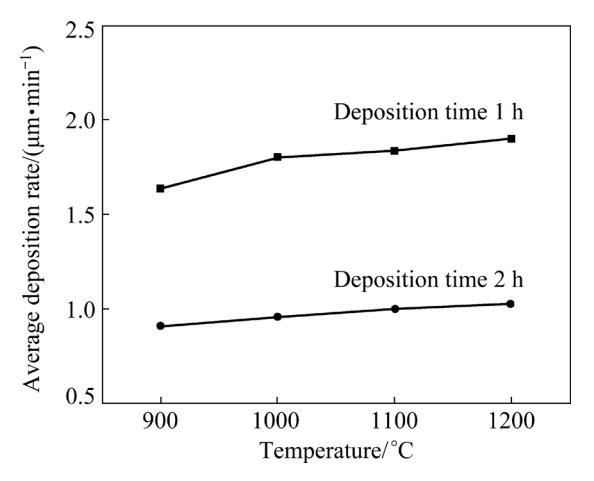


Fig. 8 Average deposition rates of SiC coatings at different deposition temperatures

3.3 Effect of deposition temperature on ablative properties of CVD-SiC coatings prepared from MS

Figure 9 shows the photos of SiC-900-1, SiC-1000-1, SiC-1100-1 and SiC-1200-1 coatings after plasma ablation of 80 s. The oxidation of the ablation center is slight with the remained coating layer. Table 1 shows the ablation resistance of SiC coatings on graphite after 80 s ablation. SiC-1000-1 shows good ablation performance, with mass ablation rate and linear ablation rate of 0.0096 mg/s and 0.3750 µm/s, respectively. Meanwhile, SiC-900-1 shows poor ablation performance, whose mass ablation rate and linear ablation rate 0.0926 mg/s and 0.9166 µm/s, respectively. The ablation resistance of SiC-1100-1 is better than that of SiC-1200-1. Deposition at too low temperatures retards the diffusion of SiC molecules, thus increasing the preparation difficulty of a SiC coating with better compactness. And the low deposition rate of SiC will cause the decrease of the preparation efficiency. However, when the deposition temperature is too high, MS decomposes too fast, which easily leads to the agglomeration of the SiC molecules. The free radicals formed during the thermal decomposition of MS are highly active, and free Si aggregates with SiC molecules during the diffusion process, the formed SiC coating has high roughness and many small pores between SiC particles (Fig. 2(d)). When the deposition temperature is too high (1100 and 1200 °C), although the crystallinity of SiC coating is increased, there is a certain amount of free Si in the coating. There is about 128% volume expansion when Si totally converts to SiO2. The stress generated by excessive volume expansion will lead to the cracking of SiC coating, thus providing a channel for oxygen molecules to diffuse to the substrate surface, and the coating protection will fail. Compared with that at 1100 °C, more free Si in SiC coating at 1200 °C leads to poor ablation resistance. Therefore, SiC prepared at 1000 °C has high crystallinity and single phase composition, and its ablation resistance is the best.

Figures 10 and 11 show the morphologies of the ablation center and the corresponding EDS data of SiC coatings after 80 s plasma ablation. The ablation center of SiC-1200-1 is composed of discontinuous molten SiO₂ particles (Area *A* in Fig. 10(b)) and Si-C-O (Area *B* in Fig. 10(b)). The

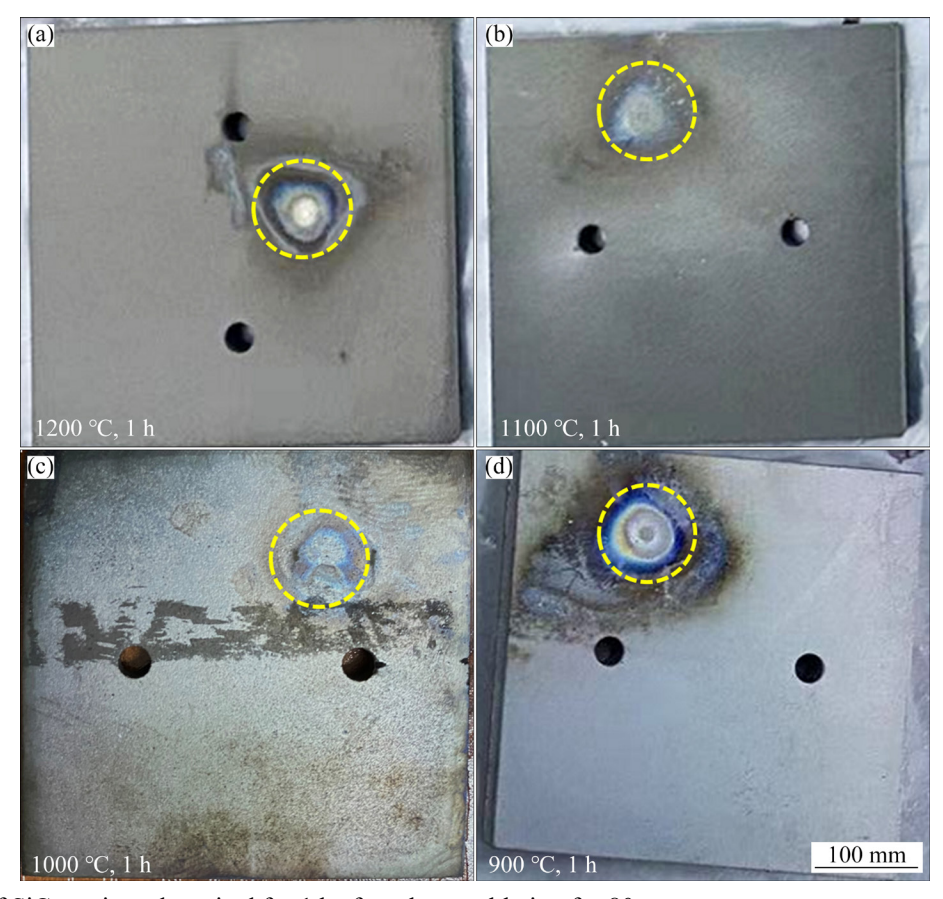


Fig. 9 Photos of SiC coatings deposited for 1 h after plasma ablation for 80 s

Table 1 Ablation rates of SiC coatings deposited for 1 and 2 h at different temperatures

Sample	Ablation time/s	$R_{\rm m}/({\rm mg\cdot s^{-1}})$	$R_{\rm l}/(\mu {\rm m}\cdot{\rm s}^{-1})$
SiC-1200-1	80	0.0513	1.0416
SiC-1100-1	80	0.0125	0.8750
SiC-1000-1	80	0.0096	0.3750
SiC-900-1	80	0.0926	0.9166
SiC-1200-2	120	0.0789	1.1911
SiC-1100-2	120	0.0250	0.9333
SiC-1000-2	120	0.0129	0.4617
SiC-900-2	120	0.1177	1.2213

ablated surface consists of a certain number of micropores. The ablation center of SiC-1100-1 is mainly composed of white granular molten SiO_2 (Area C in Fig. 10(d)) and gray Si-C-O molten film (Area D in Fig. 10(d)). The oxidized particles in Areas A and C (Fig. 10) tend to connect to form films, while some white SiO_2 small particles are included in Areas B and D (Fig. 10). Continuous molten SiO_2 in small areas (Fig. 11(a)) exist on the

ablated center of SiC-1000-1. The oxide film has good ability to fill surface defects, which can prevent the erosion and denudation of the coating. The ablation results of SiC-900-1 are shown in Figs. 11(e) and (f). Under the oxidation and erosion of the plasma flame, significant amount of consumption and loss of molten SiO₂ occur on the surface. The micropores on the ablated surface caused by the gaseous substances leaving are transformed into larger pores that cannot be healed, resulting in further accelerated failure of the SiC coating and poor ablation resistance.

Figure 12 shows the photos of SiC-900-2, SiC-1000-2, SiC-1100-2 and SiC-1200-2 coatings after 120 s plasma ablation. The ablation trace in the ablation center is not obvious without evident holes and damage, indicating that the SiC coating does not fail after 120 s ablation. Table 1 shows the ablation resistance of SiC coating on graphite. The results of ablation resistance of SiC coatings are consistent with those of Table 1. SiC-1000-2 shows good ablation performance, with mass ablation rate and linear ablation rate of 0.0129 mg/s and

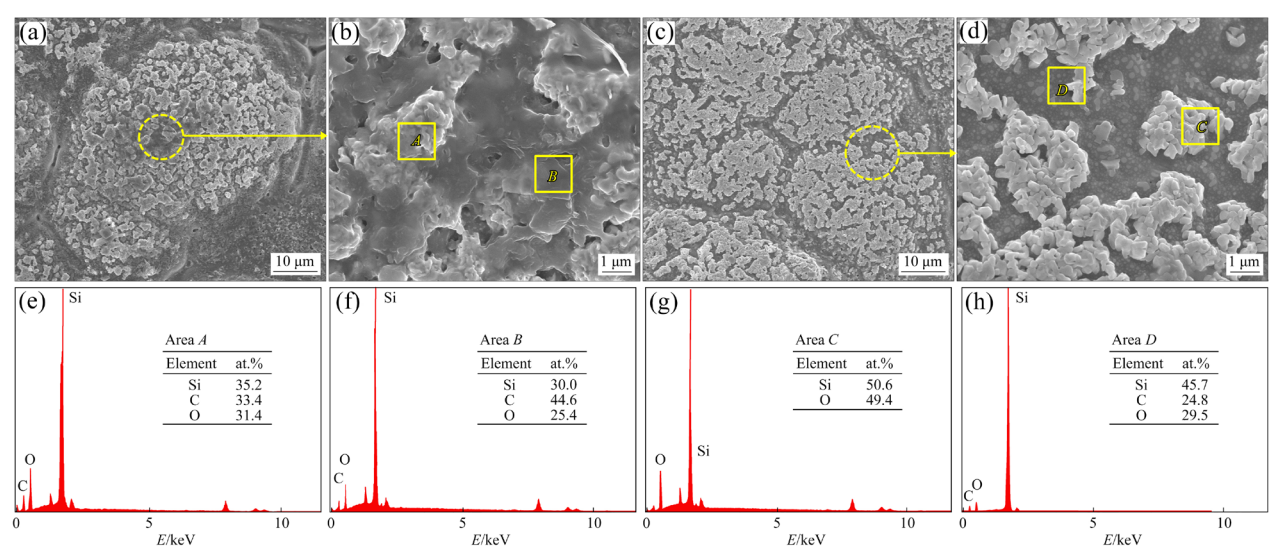


Fig. 10 SEM images (a-d) and EDS data (e-h) of ablated SiC coatings at ablation centers: (a, b, e, f) SiC-1200-1 after plasma ablation for 80 s; (c, d, g, h) SiC-1100-1 after plasma ablation for 80 s

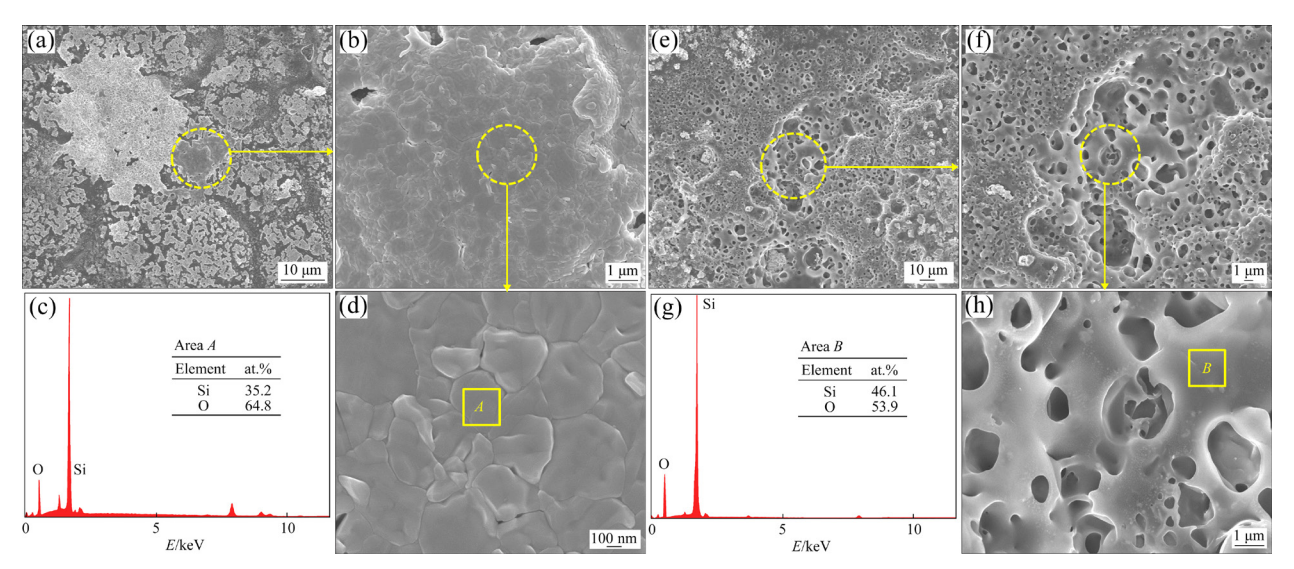


Fig. 11 SEM images (a, b, d, e, f, h) and EDS data (c, g) of ablated SiC coatings at ablation centers: (a–d) SiC-1000-1 after plasma ablation for 80 s; (e–h) SiC-900-1 after plasma ablation for 80 s

 $0.4617 \, \mu m/s$, respectively, while SiC-900-2 still shows poor ablation performance whose mass ablation rate and linear ablation rate are $0.1177 \, mg/s$ and $1.2213 \, \mu m/s$, respectively.

Figures 13 and 14 show the morphologies of the ablation center and the corresponding EDS data of SiC coatings after 120 s plasma ablation. After ablation, the surface of SiC-1200-2 is composed of discontinuous massive molten SiO₂ (Area *A* in Fig. 13(b)) and Si-C-O (Area *B* in Fig. 13(b)). Most molten SiO₂ particles are denudated on the ablated SiC-1100-2, and the ablated surface is Si-C-O molten state embedded with molten SiO₂

particles. The SiC-1000-2 with good ablation performance still has continuous molten SiO₂ oxide film (small area) on the surface. Figure 14(d) shows the local magnification of molten SiO₂ oxide film. The dense molten SiO₂ oxide film can effectively prevent the diffusion of oxygen into the coating and weaken the erosion and denudation of the coating by plasma flame. However, SiC-900-2 with poor ablation performance exhibits many micropores left on the ablated surface, which are transformed into larger pores that cannot be healed due to the departure of gaseous substances. These pores accelerate the failure of the coating.

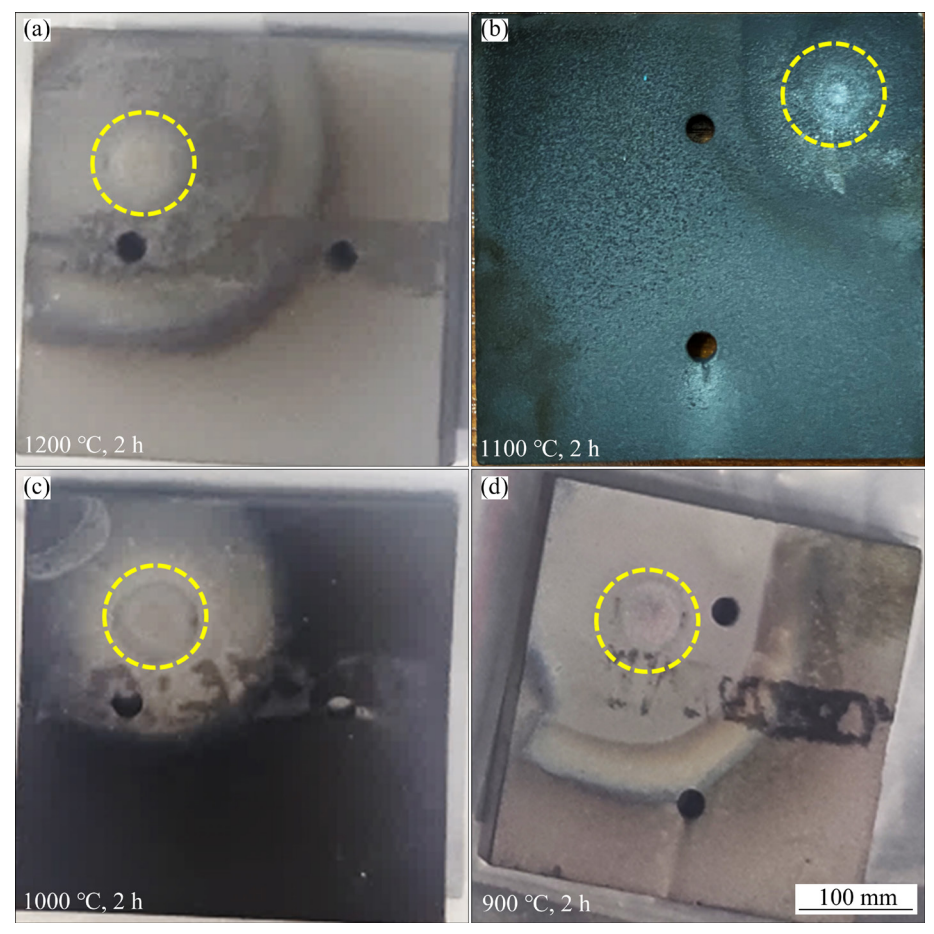


Fig. 12 Photos of SiC coatings deposited for 2 h after plasma ablation for 120 s

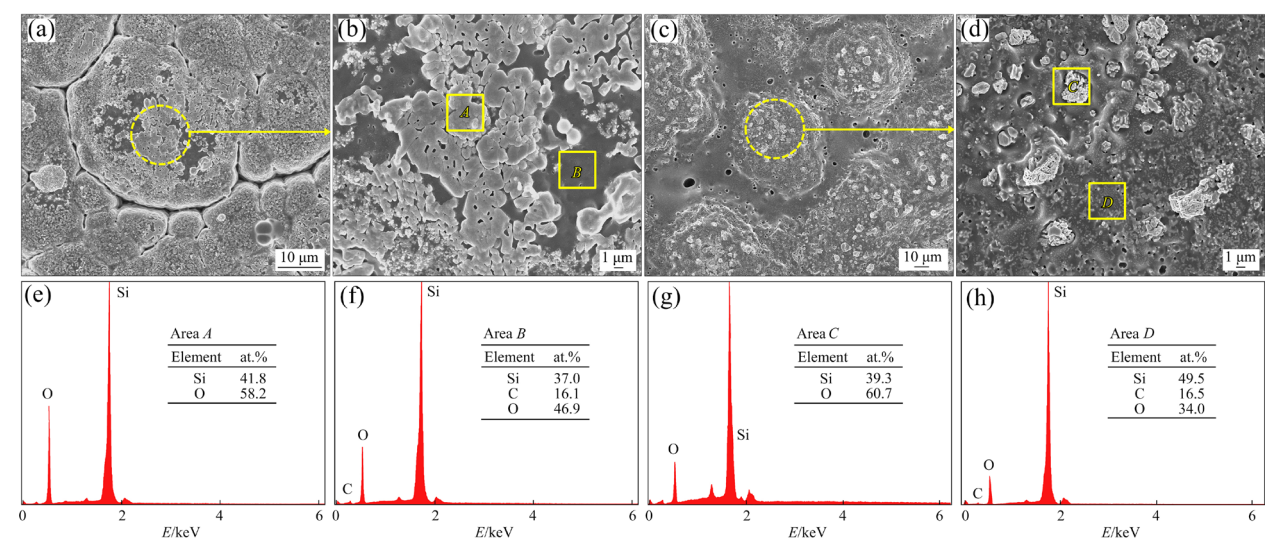


Fig. 13 SEM images (a-d) and EDS data (e-h) of ablated SiC coatings at ablation centers: (a, b, e, f) SiC-1200-2 after plasma ablation for 120 s; (c, d, g, h) SiC-1100-2 after plasma ablation for 120 s

3.4 Ablation mechanism of CVD-SiC coatings prepared from MS

The ablation of SiC coatings under plasma ablation environment is mainly thermochemical ablation and mechanical denudation. Thermochemical ablation mainly refers to the oxidation of coatings in high temperature atmosphere, and mechanical denudation refers to the physical peeling of particles and blocks of coatings and oxides under the continuous scouring of plasma flame. The reactions during the ablation of SiC coating are proposed as follows:

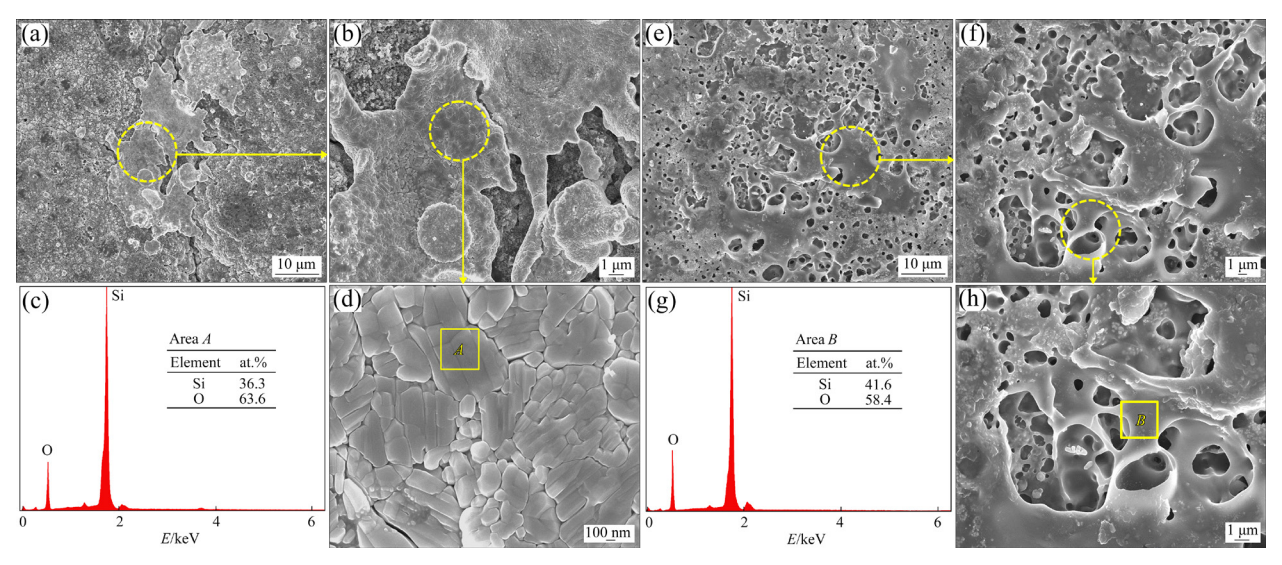


Fig. 14 SEM images (a, b, d, e, f, h) and EDS data (c, g) of ablated SiC coatings at ablation centers: (a–d) SiC-1000-2 after plasma ablation for 120 s; (e–h) SiC-900-2 after plasma ablation for 120 s

$$SiC(s)+2O_2(g) \rightarrow SiO_2(1)+CO_2(g)$$
 (14)

$$SiO_2(1) \rightarrow SiO_2(g)$$
 (15)

$$SiC(s)+2SiO_2(1)\rightarrow 3SiO(g)+CO(g)$$
 (16)

$$SiC(s)+CO_2(g) \rightarrow SiO(g)+CO(g)$$
 (17)

$$SiC(s)+CO(g)\rightarrow SiO(g)+2C(s)$$
 (18)

$$2SiO(g)+O_2(g)\rightarrow 2SiO_2(g)$$
 (19)

In the process of plasma ablation, the temperature of plasma flame in the ablation center is about 2300 °C, which is lower than the sublimation temperature of SiC (2700 °C), thus the SiC coating in the central area is mainly dominated by oxidation reaction (Reaction (14)). The part of molten SiO₂ formed during the oxidation process will vaporize (Reaction (15)) and leave the ablated surface together with other gaseous products (CO and CO₂), leaving micropores on the ablated surface, which provide channels for oxygen to erode the interior of the coating. At the same time, the molten SiO₂ generated by oxidation of SiC coating has good surface healing ability below 2300 °C. The molten SiO₂ remaining on the surface of the coating fills part of the micropores and effectively prevents the diffusion of oxygen into the inner part of the coating.

At the deposition temperature of 900 °C, the diffusion of SiC molecules is difficult due to the low deposition temperature, which affects the growth and crystallization of SiC grains and reduce

the crystallinity of SiC coating, so the SiC-900-1 has a dense structure but low crystallinity (Figs. 3(e) and 5(e)). Under the continuous scouring of plasma flame, the molten SiO_2 could not heal the micropores left on the surface due to gaseous departure, but was consumed in large quantities, resulting in a significant increase in the size and number of micropores on the ablated surface (Figs. 11(e) and (f)), thus exhibiting poor ablation resistance (Table 1).

At high deposition temperature of 1200 °C, the decomposition rate of MS is higher than the diffusion rate of SiC, which can easily lead to the agglomeration of SiC molecules. Meanwhile, the activity of free radicals formed in the process of MS thermal decomposition is too high, and the Si free radicals cannot capture the C source, so they are taken together by SiC molecules in the diffusion process, further leading to irregular cauliflower morphology of the SiC and Si particles in SiC-1200-1 (Figs. 2(a) and (b)) and SiC-1200-2 (Figs. 4(a) and (b)). In addition, high deposition temperature can decrease the rate of nucleation, resulting in significantly larger grains and a rough and porous coating structure.

The coating structure is affected by plasma flame oxidation and erosion. The agglomerated SiC molecules and Si molecules partially form molten SiO₂ remaining on the ablated surface, and a small part of the agglomerated particles are denuded due to the lack of sufficient support for the gasification

of molten SiO₂, and the denuded particles also take most of the energy out of the plasma flame. Although the coating shows poor ablation resistance, the interior of the coating is not severely oxidated. The presence of Si, whose melting point is much lower than that of SiC, reduces the high temperature ablation resistance and erosion resistance of the coating during the ablation process.

As the deposition temperature increases from 1100 to 1200 °C, the content of free Si in the increases significantly, the coating ablation resistance of SiC-1200-1 is weaker than that of SiC-1100-1. The SiC coating obtained at 1000 °C is more suitable in terms of density, roughness, coating structure and uniformity. Therefore, during the plasma ablation process, the molten SiO₂ formed on the coating surface will form a small area of continuous molten SiO2 oxide film (Figs. 11(d) and 14(d)). The oxide film has a good ability to heal surface defects, effectively preventing the diffusion of oxygen into the coating and reducing the erosion and ablation of the coating. Therefore, the coating shows good ablation resistance (Table 1).

4 Conclusions

- (1) The SiC coating obtained from the MS precursors at the deposition temperature of 1000 °C had suitable density, roughness, and uniform size of coating microstructure.
- (2) The mass ablation rate and linear ablation rate of the obtained SiC coating at the deposition temperature of 1000 °C were 0.0096 mg/s and 0.3750 μ m/s, respectively after plasma ablation at 2300 °C for 80 s.
- (3) The SiC coatings deposited at relatively low temperatures (900–1000 °C) exhibited smooth and spherical compact packing morphology, while the SiC coatings deposited at high temperatures (1100–1200 °C) possessed an irregular cauliflower morphology with significantly increasing the size of the SiC particles.
- (4) A small area of continuous molten SiO₂ oxide film could help to fill the ablative surface defects and prevent further diffusion of oxygen and ablative airflow into the coating during the ablation process.

(5) The reliable processing parameters to fabricate high quality of SiC coating were obtained and the mechanism model to understand ablation resistance for CVD SiC coating was provided, which would be beneficial to the preparation and application of SiC coatings on carbon materials for the highly focused semiconductor research filed.

Acknowledgments

This work was financially supported by the National Key R&D Program of China (No. 2021YFA0715802), and the Joint Funds of the National Natural Science Foundation of China (No. U19A2088).

References

- [1] LI He-jun, FU Qian-gang, SHI Xiao-hong, LI Ke-zhi, HU Zhi-biao. SiC whisker-toughened SiC oxidation protective coating for carbon/carbon composites [J]. Carbon, 2006, 44(3): 602–605.
- [2] LIU Hu, LI Long-biao, YANG Jin-hua, ZHOU Yi-ran, AI Ying-jun, QI Zhe, GAO Ye, JIAO Jian. Characterization and modeling damage and fracture of prepreg-MI SiC/SiC composites under tensile loading at room temperature [J]. Applied Composite Materials, 2022, 29(3): 1167–1193.
- [3] YANG Xin, HUANG Qi-zhong, SU Zhe-an, CHANG Xin, CHAI Li-yuan, LIU Chun-xuan, XUE Liang, HUANG Dong. Resistance to oxidation and ablation of SiC coating on graphite prepared by chemical vapor reaction [J]. Corrosion Science, 2013, 75: 16–27.
- [4] FU Qian-gang, LI He-jun, SHI Xiao-hong, LI Ke-zhi, WANG Chuang, HUANG Min. Double-layer oxidation protective SiC/glass coatings for carbon/carbon composites [J]. Surface and Coatings Technology, 2006, 200(11): 3473-3477.
- [5] FU Qian-gang, LI He-jun, SHI Xiao-hong, LI Ke-zhi, SUN Guo-dong. Silicon carbide coating to protect carbon/carbon composites against oxidation [J]. Scripta Materialia, 2005, 52(9): 923–927.
- [6] KATOH Y, SNEAD L L, SZLUFARSKA I, WEBER W J. Radiation effects in SiC for nuclear structural applications [J]. Current Opinion in Solid State and Materials Science, 2012, 16(3): 143-152
- [7] SONG J T, MASHIKO H, KAMIYA M, NAKAMINE Y, OHTOMO A, IWASAKI T, HATANO M. Improved visible light driven photoelectrochemical properties of 3C-SiC semiconductor with Pt nanoparticles for hydrogen generation [J]. Applied Physics Letters, 2013, 103(21): 213901.
- [8] HU Xiang-long, HUANG Min, KONG Ni-zao, HAN Fei, TAN Rui-xuan, HUANG Qi-zhong. Enhancing the electrical insulation of highly thermally conductive carbon fiber powders by SiC ceramic coating for efficient thermal interface materials [J]. Composites (Part B): Engineering, 2021, 227: 109398.

- [9] ZENG Kuan-hong, MA Qing-song, GU Xing-yu. Effects of SiC interfacial coating on mechanical properties of carbon fiber needled felt reinforced sol-derived Al₂O₃ composites [J]. Transactions of Nonferrous Metals Society of China, 2020, 30(2): 463–471.
- [10] ZHANG Zhen-bang, LIAO Mei-zhan, LI Mao-hua, LI Lin-hong, WEI Xian-zhe, KONG Xiang-dong, XIONG Shao-yang, XIA Jun-cheng, FU Li-qin, CAI Tao, PAN Zhong-bin, LI Hao-nan, HAN Fei, LIN Cheng-te, NISHIMURA K, JIANG Nan, YU Jin-hong. Enhanced thermal conductivity for polydimethylsiloxane composites with core—shell CFs@SiC filler [J]. Composites Communications, 2022, 33: 101209.
- [11] WU Shou-jun, CHENG Lai-fei, ZHANG Li-tong, XU Yong-dong. Oxidation behavior of 2D C/SiC with a multi-layer CVD SiC coating [J]. Surface and Coatings Technology, 2006, 200(14/15): 4489–4492.
- [12] CHENG Lai-fei, XU Yong-dong, ZHANG Li-tong, YIN Xiao-wei. Preparation of an oxidation protection coating for C/C composites by low pressure chemical vapor deposition [J]. Carbon, 2000, 38(10): 1493–1498.
- [13] JACOBSON N S, ROTH D J, RAUSER R W, CAWLEY J D, CURRY D M. Oxidation through coating cracks of SiC-protected carbon/carbon [J]. Surface and Coatings Technology, 2008, 203(3/4): 372–383.
- [14] CHENG Lai-fei, XU Yong-dong, ZHANG Li-tong, LUAN Xin-gang. Oxidation and defect control of CVD SiC coating on three-dimensional C/SiC composites [J]. Carbon, 2002, 40(12): 2229–2234.
- [15] PIERSON H O. Handbook of chemical vapor deposition: Principles, technology and application [M]. New York, USA: Noyes Publications, 1999: 34–39.
- [16] LU Cui-ying, CHENG Lai-fei, ZHAO Chun-nian, ZHANG Li-tong, YE Fang. Effects of residence time and reaction conditions on the deposition of SiC from methyltrichlorosilane and hydrogen [J]. International Journal of Applied Ceramic Technology, 2012, 9(3): 642–649.
- [17] WU Qiang, YU Shu, ZHONG Hui, LI Xiao, XIAO Tao, LIU Li-hong, GUO Xiao-ning, LI Yun-ping, NIE Yan. Preparation of silicon carbide coating by chemical vapor deposition by using hexamethyldisilylamine precursor [J]. Surface and Coatings Technology, 2018, 334: 78–83.
- [18] YAN Xiu-tian, XU Yong-dong. Chemical vapour deposition: An integrated engineering design for advanced materials [M]. London: Springer Science & Business Media, 2010: 2–10.
- [19] CHOY K L. Chemical vapour deposition of coatings [J]. Progress in Materials Science, 2003, 48(2): 57–170.
- [20] VAHLAS C, CAUSSAT B, SERP P, ANGELOPOULOS G N. Principles and applications of CVD powder technology

- [J]. Materials Science and Engineering: R, 2006, 53(1/2): 1-72
- [21] OUESLATI I, HECHMI M, JEBARI E, BACCARI K, KERKENI B. Rate coefficients and kinetic isotope effects of the abstraction reaction of H atoms from methylsilane [J]. Molecular Physics, 2016, 114(22): 3396–3406.
- [22] ABYZOV A M, SMIRNOV E P. Kinetics of SiC chemical vapor deposition from methylsilane [J]. Inorganic Materials, 2000, 36(9): 884–890.
- [23] GOLECKI I, REIDINGER F, MARTI J. Single-crystalline, epitaxial cubic SiC films grown on (100) Si at 750 °C by chemical vapor deposition [J]. Applied Physics Letters, 1992, 60(14): 1703–1705.
- [24] NEUDORFL P S, STRAUSZ O P. Pyrolysis of monomethyland dimethylsilane: The role of molecular and radical processes [J]. The Journal of Physical Chemistry, 1978, 82(2): 241–242.
- [25] JOHNSON A D, PERRIN J, MUCHA J A, IBBOTSON D E. Kinetics of silicon carbide CVD: Surface decomposition of silacyclobutane and methylsilane [J]. The Journal of Physical Chemistry, 1993, 97(49): 12937–12948.
- [26] SANCHEZ E C, SIBENER S J. Low-temperature growth of epitaxial β-SiC on Si (100) using supersonic molecular beams of methylsilane [J]. The Journal of Physical Chemistry B, 2002, 106(33): 8019–8028.
- [27] OHSHITA Y. Reactants in SiC chemical vapor deposition using CH₃SiH₃ as a source gas [J]. Journal of Crystal Growth, 1995, 147(1/2): 111–116.
- [28] RING M A, O'NEAL H E, RICKBORN S F, SAWREY B A. Kinetics of the high-temperature thermal decomposition of silanes and alkylsilanes [J]. Organometallics, 1983, 2(12): 1891–1894.
- [29] SAWREY B A, O'NEAL H E, RING M A, COFFEY D Jr. The gas-phase decomposition of methylsilane. Part I: Mechanism of decomposition under shock-tube conditions [J]. International Journal of Chemical Kinetics, 1984, 16(1): 7–21.
- [30] SAWREY B A, O'NEAL H E, RING M A. The gas-phase decomposition of methylsilane. Part II: Mechanisms of decomposition under static system conditions [J]. International Journal of Chemical Kinetics, 1984, 16(1): 22–30.
- [31] SAWREY B A, O'NEAL H E, RING M A, COFFEY D Jr. The gas-phase decomposition of methylsilane. Part III: Kinetics [J]. International Journal of Chemical Kinetics, 1984, 16(1): 31–39.
- [32] ZHANG Chang-rui, LIU Rong-jun, CAO Ying-bin. Effects of deposition temperature on the microstructures of SiC coatings by CVD [J]. Journal of Inorganic Materials, 2007, 22(1): 153–158. (in Chinese)

沉积温度对甲基硅烷化学气相沉积 SiC 涂层显微组织和烧蚀性能的影响

胡祥龙1,罗骁1,杨鑫1,谭瑞轩2,黄启忠1

- 1. 中南大学 轻质高强结构材料国家级重点实验室,长沙 410083;
- 2. 湖南大学 湖南省先进炭材料及应用技术湖南省重点实验室,长沙 410082

摘 要:以甲基硅烷(MS)为气源,采用化学气相沉积方法于不同温度下在石墨表面制备 SiC 涂层,并系统研究温度对 SiC 涂层的沉积速率、显微组织和抗烧蚀性能的影响规律。实验结果表明:当沉积温度为 1000 ℃时,以 MS 为气源的 SiC 涂层的沉积速率为 50~120 μm/h,远高于以甲基三氯硅烷为气源的沉积速率(5~10 μm/h)。当沉积温度较低(900~1000 ℃)时,以 MS 为气源所制备的 SiC 涂层整体光滑、平整,呈球形紧密堆积形貌;沉积温度较高(1100~1200 ℃)时, SiC 涂层呈不规则菜花状颗粒堆积形貌,且微晶尺寸明显增大;当沉积温度为 1000 ℃时,SiC 涂层具有合适的致密性、粗糙度以及尺寸均匀的显微组织,同时,该涂层经 2300 ℃等离子烧蚀 80 s 后,其质量烧蚀率和线性烧蚀率分别为 0.0096 mg/s 和 0.3750 μm/s,显示优异的抗烧蚀性能。本研究为以 MS 为气源的化学气相沉积法制备 SiC 涂层提供一定的理论基础和技术支撑。

关键词: 甲基硅烷; 化学气相沉积; SiC 涂层; 沉积温度; 显微组织; 烧蚀性能

(Edited by Wei-ping CHEN)